Original Article

# Comparative assessment of the accuracy of maximum likelihood and correlated signal enhancement algorithm positioning methods in gamma camera with large square photomultiplier tubes

**Behnoosh Teimourian Fard[1,2], Mojtaba Shamsaei Zafarghandi[1]**

[1]Department of Energy Engineering and Physics, Amirkabir University of Technology, Tehran, Iran
[2]Research Center for Molecular and Cellular Imaging, Tehran University of Medical Sciences, Tehran, Iran

(Received 29 September 2018, Revised 14 January 2019, Accepted 14 January 2019)

## ABSTRACT

**Introduction:** The gamma cameras, based on scintillation crystal followed by an array of photomultiplier tubes (PMTs), play a crucial role in nuclear medicine. The use of square PMTs provides the minimum dead zones in the camera. The camera with square PMTs also reduces the number of PMTs relative to the detection area. Introduction of a positioning algorithm to improve the spatial resolution in the detector with square PMT have been of interest in recent years.

**Methods:** In this study, the maximum-likelihood and correlated signal enhancement positioning methods were implemented in a camera with square PMTs. The developed camera consists of 3/8" thick monolithic NaI(Tl) crystal coupled to the array of 76mm sized PMTs. The comparison is based on measuring full width at half maximum (FWHM) and standard deviation of FWHM of point sources in a 15×15 grid of samples with 2-mm grid spacing, produced using MLE and CSE positioning methods.

**Results:** The intrinsic spatial resolution in ($x$, $y$) directions was (3.8, 3.8), (4.3, 4.5) mm for CSE and MLE methods respectively. Also, the standard deviations was almost the same in both methods (0.5 and 0.6 for CSE and MLE respectively). Although by applying MLE method, the resolution degrades by 16% but the produced image introduced acceptable quality.

**Conclusion:** The results show the MLE method presented acceptable performance in comparison to CSE method as reference in the detector with large square PMTs. Note that the MLE method does not require any linearity correction process because it can estimate the exact position of events.

**Key words:** Gamma camera; Square photomultiplier tubes; Position estimation; Maximum likelihood estimation; Correlated signal enhancement

**Iran J Nucl Med 2019;27(2):81-86**
Published: July, 2019
http://irjnm.tums.ac.ir

**Corresponding author:** Mojtaba Shamsaei Zafarghandi, Department of Energy Engineering and Physics, Amirkabir University of Technology, Tehran, Iran. E-mail: pysham@aut.ac.ir

## INTRODUCTION

The gamma camera based on the scintillation materials has been introduced by Anger et al. to obtain a map of the distribution of radionuclide within the body after it has been administered to body (e.g., by intravenous injection) [1]. The most common architecture of the camera includes scintillation crystal coupled to light guide, read out by an array of photo multiplier tubes (PMTs) [2, 3]. The emitted gamma photons from distributed radionuclide interact with the scintillation crystal and produce optical photons and further are converted to electrical signals by PMTs. These signals used to estimate the 2D position of the interaction and the deposited energy in the crystal. In a large area camera, the dominant factor which influences image quality and cost of the detector is the selection of the PMTs with appropriate size and shape. With keeping in mind that the common scintillation crystal has rectangular shape, the square PMT is the most appropriate type, because of covering efficiently the edges of the rectangular crystal compared to the hexagonal or circular types [4].

The position calculation algorithm in any gamma camera is an important issue that highly influence the image quality. However, it is well known that the efficiency of the positioning methods completely depends on the size and shape of PMTs.

The aim of the study is applying and evaluating the method from statistical estimation theory, particularly maximum-likelihood estimation (MLE) method [5-8], in the case of using the square large PMTs in the scintillation camera. For assessing the performance of the MLE method, its experimental results compared with the correlated signal enhancement (CSE) algorithm that is commonly used [4, 9].

## METHODS

### Scintillation camera

We have developed a rectangular gamma camera consists of a large area NaI(Tl) crystal, and an array of PMTs to evaluate the MLE positioning methods experimentally. The NaI(Tl) crystal with 40×25 $cm^2$ area and 9.5 mm thickness attached to the light guide with 18 mm thickness is used in the camera. A thin aluminum plate (0.4 mm) is used as the entrance window also the entrance and side faces is coated with a white epoxy compound as reflector. The array of 6×4 square PMTs with 76×76 $mm^2$ area (R6237, Hamamatsu, Japan) is placed on the light guide at the back of the crystal. Since the array should be optically coupled with the crystal, a home-made silicon-based glue is developed to be transparent in addition to have good adhesive properties [10]. A high voltage of -900 V was applied to all the 24 PMTs. All camera components are shielded from external light in a ferrous housing. Also the lead is used to shield the camera from gamma ray except the face of the detector. The readout of the detector is the same as described in our previous work [10].

The MLE and CSE positioning methods are applied to estimate the 2D position of interaction in the detector, and then the intrinsic spatial resolution of each method is obtained. Each estimation method is evaluated by FWHM and variance of the estimated positions of point sources in a 15×15 grid with 2-mm grid spacing placed on the detector surface. FWHM and variance both directly impact the intrinsic spatial resolution. In the following implementation of both methods clarified in more detail.

### Data acquisition and calibration process

In this study, we need to have 2D calibration data, acquired with a well-collimated beam of gamma rays normal to the face. So a collimated Tc-99m source is scanned in a 75×75 grid pattern with 2-mm grid spacing across the camera face. It should be noted that the mean detector response function (MDRF) are interpolated to 149×149 samples with 1-mm grid spacing. The acquired data covered almost a quarter of detector area (150×150 $mm^2$). More than 10,000 counts acquired in every calibration point and it lasts about 10 seconds.

This calibration process provides the mean detector response function (MDRF) of the gamma camera through calculating the average response of each PMT in the detector as a function of the position of the calibration point on the detector face. The measured MDRF is included all optical and electronic properties of the gamma camera [5, 11].

A source holder with opening hole with 1.0 mm diameter was used to simulate the point source (Figure 1).

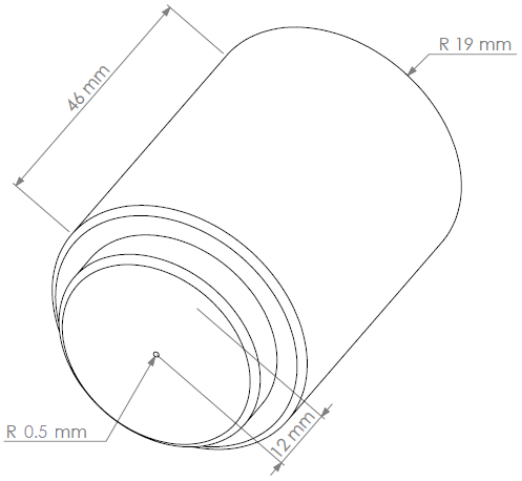


**Fig 1.** The drawing of source holder that is used to make the point source.

The source holder should be moved on the different positions on the detector surface to expand the evaluation of spatial resolution to entire surface of the camera. For this purpose, a moving mechanism is implemented as shown in Figure 2, that provides movement of source holder in the both *x* and *y* directions of the detector plane with 1 mm precision.

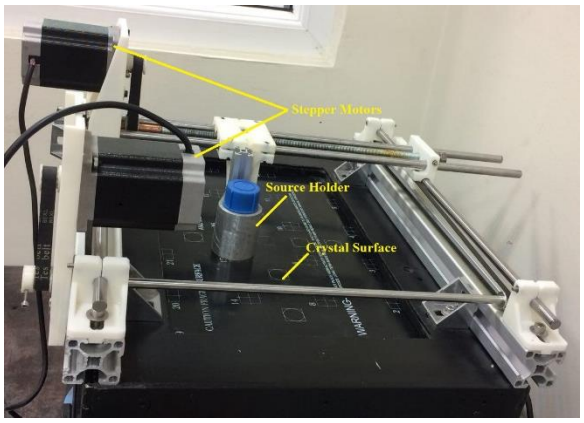


**Fig 2.** The equipment that is designed and developed to provide the movement of source holder in x or y direction in 1 mm precision.

## Correlated signal enhancement (CSE) method

In this method, the column and row summations are first obtained, and then simple 1D center of mass (COM) is individually implemented for each direction (x and y) to estimate the position of interaction in 2D plane [4]. Also, a nonlinear correction function should be applied on the column and row summation values to achieve a better intrinsic spatial resolution and linearity.

$$\hat{x} = \frac{\sum_i x_{col_i}\, wf\left(col_{nor\,i}\right) col_i (\geq S_{min})}{\sum_i col_i\,(\geq S_{min})}, \qquad (1)$$

$$col_i = \sum_j S_{ij}\,, \qquad col\_nor_i = \frac{\sum_i S_{ij}}{\sum_i \sum_j S_{ij}}$$

$$\hat{y} = \frac{\sum_j y_{row_j}\, wf\left(row_{nor\,j}\right) row_j (\geq S_{min})}{\sum_j row_j\,(\geq S_{min})}, \qquad (2)$$

$$row_j = \sum_i S_{ij}\,, \qquad row\_nor_j = \frac{\sum_i S_{ij}}{\sum_i \sum_j S_{ij}}$$

where $i$ and $j$ is the number of columns and row respectively, the $S_{ij}$ is the signal of PMT in $i^{th}$ column and $j^{th}$ row and the *wf* is a Gaussian-based correction function which modifies the signal of each column and row [10]. The *wf* function depends on geometric of detector and it has to customize for each detector. The function is optimized for the presented detector in our previous work [10]:

$$wf(x) = exp\left[-\frac{((x-0.3)\text{^}2)}{2(0.5)\text{^}2}\right] \qquad (3)$$

The *wf* function produces a weighted factor that weakens very large and very small signals regarding the column (row) summation. It should be noted that the very small signals have poor signal-to-noise ratio (SNR) and also there is not much valuable information to estimate position of interaction in the very large signals. Also we applied a threshold level 2% (represented $S_{min}$ in the equation (1) and (2)) as the same manner of the conventional canter of mass methods [8, 12].

## MDRF processing

The MDRF data set is applied to calculate the means of the signal output of each PMT as a function of the point source location. The sample means should be calculated for the events that set in the photo peak. For this purpose, first of all the image of each calibration point is obtained using CSE method (described in the section 0.), then a Gaussian function is fitted to the photo peak in the obtained image, finally all events outside of the six standard deviations (SD) of the fitted function discards from the data. The means of PMT signals are calculated for the residual events and save as the response of each PMT as a function of the position on the detector face.

## MLE method

In this study we considered the statistics of the gamma ray detection is approximately Poisson and therefore the number of electron produced at each PMT is also Poisson by the binomial-selection theorem [11, 13]. If $n_i$ denoted as the output signal of the $i^{th}$ PMT, then the Poisson probability law on $n_i$ can described as:

$$p(n_i|r_{int}, E_{int}) = exp(-n_i)\left(\frac{\bar{n}_i^{n_i}}{n_i!}\right), \qquad (4)$$

$$i = \{1,2,\ldots,24\}$$

Where $\mathbf{r}_{int}$ is the 2D interaction location in the scintillation crystal, and $E_{int}$ is the energy deposited in the interaction and 24 is the number of PMT in the developed camera. Since the PMT output signals are statistically independent, the multivariate probability law can be applied for a set of $n_i$ , i = (1,2,…,24), associated with any single gamma ray event in the modular detector:

$$p(\boldsymbol{n}|\boldsymbol{r}_{int}, E_{int}) = \prod_{i=1}^{24} exp(-n_i)\left(\frac{\bar{n}_i^{n_i}}{n_i!}\right), \qquad (5)$$

$$i = \{1,2,\ldots,24\}$$

Where $\boldsymbol{n}$ is a vector of the PMT signals, ($n_1$, $n_2$, …,$n_i$). This model originated with the work of Barret in 2005 and referred as the scaled Poisson model [11]. With substituting *ni* (**r**int, *E*int ) that calculated from calibration process (described in the section 0 and 0.) the MLE method can estimate the position and energy of any event with the the vector **n**:

$$\left(\hat{\boldsymbol{r}}_{int}, \hat{E}_{int}\right) = \arg\max p\left(\boldsymbol{n}|\boldsymbol{r}_{int}, E_{int}\right) \qquad (6)$$

If we assume the collimated source that used in the calibration process is monoenrgetic, we will have:

$$\ln p\left(\{n_i\}|x,y\right) = \sum_{i=1}^{24}\left(n_i \ln \bar{n}_i(x,y) - \bar{n}_i(x,y)\right) - \sum_{i=1}^{24} \ln(n_i!) \qquad (7)$$

The last term of the above equation is independent from (x,y) and so can be considered as constant in searching ML solution. It should be noted that it is relevant for the likelihood windowing described in the section 0. Finally the ML position for the interaction location is estimated from:

$$(\hat{x}_{ML}, \hat{y}_{ML}) = \arg\max[\ln p(\boldsymbol{n}|x,y)] \qquad (8)$$

## Likelihood windowing

There are several technique to reject the scattered interactions in the MLE method [14-16]. Since we already compute the last term in (10), the likelihood windowing (LW) is implemented in this work. For this purpose, in the first step the position-independent likelihood thresholding ($L_0$(x,y)) is calculated using the calibration data, then every event that the maximized likelihood can satisfy the following condition, is accepted.

$$p(\boldsymbol{n}|\hat{x}_{ML}, \hat{y}_{ML}) > L_0(\hat{x}_{ML}, \hat{y}_{ML}) \qquad (9)$$

For computing $L_0$(x,y), First the log-likelihood is calculated for each calibration point using (10) and then the maximum of the likelihood values is found and finally 85% of this maximum is considered the likelihood thresholding in corresponding position of calibration point (x,y). Histogram of the log-likelihood for all events correspond to one of calibration point is presented in (Figure 3).

## Comparison strategy

A grid pattern of 15×15 with 10-mm grid spacing across the camera face is used to evaluate the MLE method. All of the 225 point sources are acquired in the same manner of the calibration acquisition.

The intrinsic spatial resolution in combination with standard deviation of the MLE method are reported and compared to the corresponding value of The CSE one as the reference. The full width at half maximum (FWHM) of a point source that placed on the detector surface was calculated to obtain the intrinsic spatial resolution.

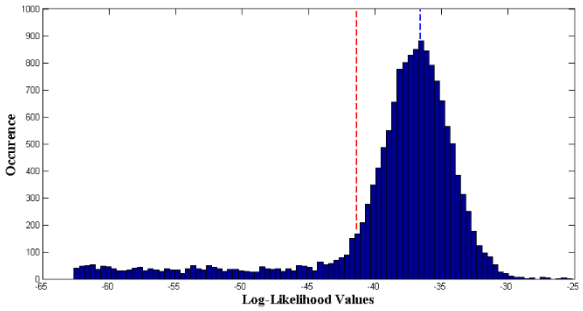


**Fig 3.** Histogram of the log-likelihood for all events correspond to one of calibration point. The blue line indicate the maximum of the likelihood and the red line demonstrates the likelihood threshold. The location source is (20, 20)..

Note that due to the symmetry, we considered only a quarter of the detector. Also for conversion of the pixel size to millimeter in reporting the FWHM, we used the adjacent images that the physical distance between the point source locations of them is 10-mm. Then differences between the peak of point source locations in each acquired image was calculated in pixel (*P*) and the conversion factor (*cf*), was obtained from:

$$cf(pixel\ to\ millimeter) = \frac{10}{P}\left({}^{mm}/_{pixel}\right) \qquad (10)$$

It should be noted that pixel size depends on the position of the point source, because all of the measurements are performed before the linearity correction process. Therefore, the pixel size should be calculated for every point individually.

## RESULTS

The Sample histogram of the signals from one PMT for one grid point of the MDRF calibration is shown in Figure 4.

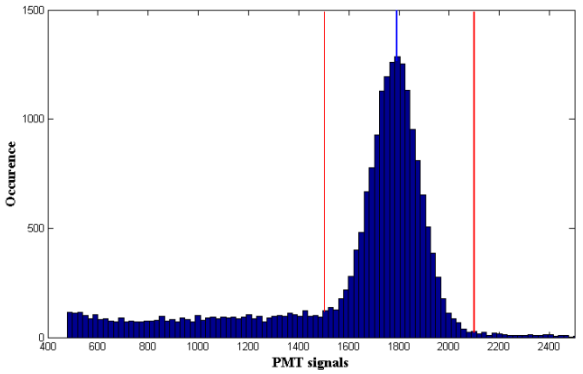


**Fig 4.** The Sample histogram of the signals from one PMT for one grid point of the MDRF calibration. The red vertical lines show the lower and upper limits of the applying Gaussian filter. The blue vertical line indicates the mean of the photopeak events. The location of the source is on the center of the PMT.

The red vertical lines show the lower and upper limits of the applying Gaussian filter. The blue vertical line indicates the mean of the photopeak events. The shown mean is calculated for each PMT in all of grid points (149×149) to compute the filtered MDRF. The filtered is used to estimate the interaction position in the MLE method.

The acquired image from the 15×15 grid that estimated using both the MLE and CSE methods and represented in Figure 5.

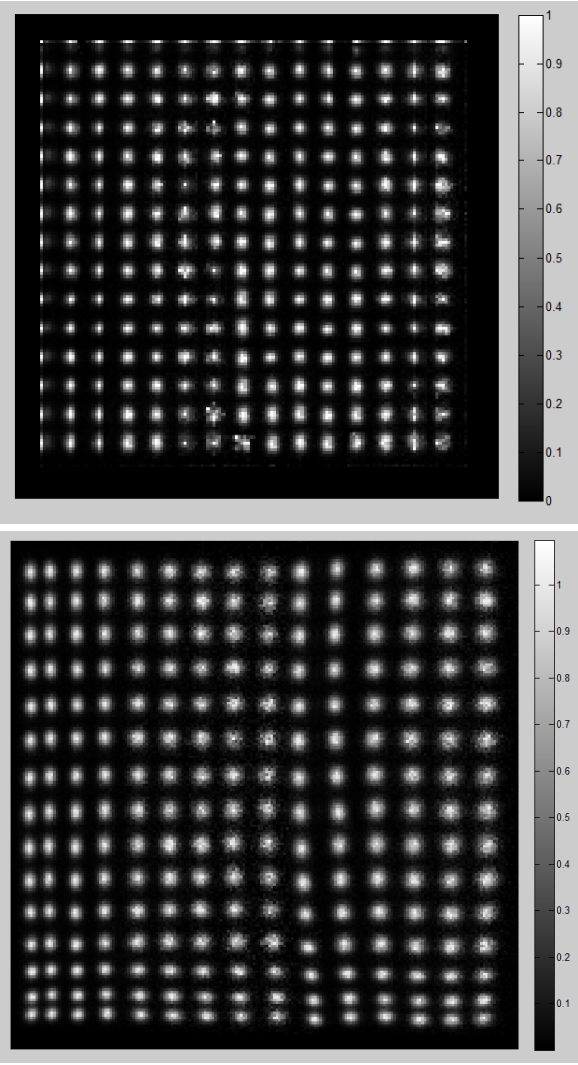

**Fig 5.** The acquired image from the 15×15 grid that estimated using (above) the MLE and (below) CSE methods.

The MLE estimates the position of point sources with more accuracy in comparison with CSE method. Also for quantitative analysis, we presented the intrinsic resolutions in combination with standard deviations for the both method in Table 1.

As shown in Table 1, although the MLE method degrade the intrinsic resolution by 16% in comparison the CSE method, but the method remains acceptable for using in the gamma camera.

**Table 1:** The mean FWHMs and SDs of point sources in a grid of 15×15, covered 150×150 $mm^2$ area of the detector, obtained from MLE and CSE positioning methods in both direction of x,y.

| Positioning Method | CSE | MLE |
|---|---|---|
| x-direction (mean ±SD) mm | 3.8±0.4 | 4.3±0.7 |
| y-direction (mean ±SD) mm | 3.8±0.6 | 4.5±0.6 |

The flood image also is acquired using the point source of Tc-99m with strength of 300 µCi that placed 2m away from camera face. Each camera had 25000 cps on average while the background was about 500 cps/camera. The integration time was 35 minutes in order to acquire about 500 events per pixel of image if the image size is considered 512×512.

## DISCUSSION

As shown in Figure 4, the MLE method can estimate the position of point sources with excellent accuracy so the MLE method does not need any linearity calibration process to match the physical location of the events with the position in the image.

Our results are similar to the previous work implementing the MLE method in a detector with monolithic NaI(Tl) crystal and a 3 × 3 array of PMTs resulting good spatial resolution with no need for distortion correction in comparison with Anger algorithm [5].

However the spatial resolution of MLE method is poorer than the CSE method but these values are appropriate for the scintillation camera and are comparable to other commercial systems as shown in Table 2.

## CONCLUSION

We developed a rectangular gamma camera with combination of an array of 6×4 square PMTs then we applied the MLE positioning method on the developed detector and evaluated the performance of the method using comparing the image quality and intrinsic resolution to CSE method as reference. The MLE technique presented acceptable performance while using the detector equipped with the large square PMTs. The main disadvantage of the method is the long calibration process. Its major advantage, is the independence from any linearity calibration process. The linearity process is replaced by the long calibration process. We aim to expand the MLE method using the implementation of maximum a posteriori (MAP) technique in the developed detectors.

**Table 2:** Intrinsic spatial resolution of developed detector in comparison with three commercial gamma cameras.

| Specifications | Developed Detector | Discovery NM/CT 670 | Millennium MG | Philips BrightView |
|---|---|---|---|---|
| Crystal Thickness (mm) | 9.5 | 9.5 | 8.5 | 9.5 |
| PMT Shape | Square | Round | Square | Round |
| Detector Field of View ($cm^2$) | 37×22 | 54×40 | 37×52 | 54×40.6 |
| Intrinsic Spatial Resolution (mm) | 3.8 (CSE) 4.4 (MLE) | 3.8 | 3.9 | 3.3 |

In this technique, prior knowledge of the desired parameters are applied by forming MAP estimator to improve the accuracy of the estimation process [6, 17]. Also, we are planning to apply the neural network theory to estimate the position of interaction in the future work [18-20].

## Acknowledgments

This work was supported under grant number 32047, Tehran University of Medical Sciences, Tehran, Iran, and Amirkabir (Tehran Polytechnic) University of Technology, Tehran, Iran.

## REFERENCES

1. Anger HO. Scintillation camera. Rev Sci Instrum. 1958;29:27-33.
2. Peterson TE, Furenlid LR. SPECT detectors: the Anger camera and beyond. Phys Med Biol. 2011;56:R145.
3. Pani R, Pellegrini R, Soluri A, De Vincentis G, Scafe R, Pergola A. Single photon emission imaging by position sensitive PMT. Nucl Instrum Methods Phys Res A. 1998;409:524-528.
4. Flower MA. Webb's physics of medical imaging. 2nd ed. CRC Press; 2012.
5. Barrett HH, Hunter WC, Miller BW, Moore SK, Chen Y, Furenlid LR. Maximum-likelihood methods for processing signals from gamma-ray detectors. IEEE Trans Nucl Sci. 2009;56:725-735.
6. Gray RM Macovski A. Maximum a posteriori estimation of position in scintillation cameras. IEEE Trans Nucl Sci. 1976;23:849-852.
7. Moore S, Hunter W, Furenlid L, Barrett H. Maximum-likelihood estimation of 3D event position in monolithic scintillation crystals: Experimental results. IEEE Nucl Sci Symp Conf Record, 2007.
8. Galasso M, Fabbri A, Borrazzo C, Cencelli VO, Pani R. A theoretical model for fast evaluation of position linearity and spatial resolution in gamma cameras based on monolithic scintillators. IEEE Trans Nucl Sci. 2016;63:1386-1398.
9. Jansen FP, Binnie DM. Signal processing in scintillation cameras for nuclear medicine. Patent 5,504,334, 1996.
10. Zeraatkar N, Sajedi S, Fard BT, Kaviani S, Akbarzadeh A, Farahani MH, Sarkar S, Ay MR. Development and calibration of a new gamma camera detector using large square Photomultiplier Tubes. J Instrum. 2017;12:P09008.
11. Barrett HH. Detectors for small-animal SPECT II, statistical limitations and estimation methods. In: Kupinski MA, Barrett HH. Small-animal SPECT imaging. Boston, MA: Springer; 2005.p. 49-86.
12. Anger HO. Scintillation camera with multichannel collimators. J Nucl Med.1964;5:515-531.
13. Barrett HH, Myers KJ. Foundations of image science. John Wiley & Sons; 2013.
14. Chen JC, Barrett HH. Likelihood window, energy window, and Bayesian window for scatter rejection in gamma cameras. IEEE Nucl Sci Symp Med Imaging Conf. (NSS/MIC), 1993.
15. Chen JC: Modular gamma cameras: Improvements in scatter rejection, and characterization and initial clinical application. PhD thesis. University of Arizona, Committee on Optical Science (Graduate); 1995.
16. ChenJC. Scatter rejection in modular gamma cameras for use in dynamic 3D SPECT brain imaging system. Comput Med Imaging Graph. 1997 Sep-Oct;21(5):283-91.
17. Fessler JA, Rogers WL, Clinthorne NH, Robust maximum-likelihood position estimation in scintillation cameras. IEEE Nucl Sci Symp Med Imaging Conf. (NSS/MIC),1991.
18. Bruyndonckx P, Léonard S, Tavernier S, Lemaître C, Devroede D, Wu Y, Krieguer M. Neural network-based position estimators for PET detectors using monolithic LSO blocks. IEEE Trans Nucl Sci. 2004;51(5):2520-2525.
19. Talat D Guvenis A. Artificial neural network based positioning algorithm for PEM imaging. 14th National Biomedical Engineering Meeting; 2009 May 20-22; Balcova, Izmir, Turkey.
20. Conde P, Iborra A, González A, Hernández L, Bellido P, Moliner L, Rigla JP, Rodríguez-Álvarez MJ, Sánchez F. Determination of the interaction position of gamma photons in monolithic scintillators using neural network fitting. IEEE Trans Nucl Sci. 2016;63(1):30-36.